

# Robust Strategies for Affirming Kramers-Henneberger Atoms

Pei-Lun He,\* Zhao-Han Zhang, and Feng He†

Key Laboratory for Laser Plasmas (Ministry of Education) and Department of Physics and Astronomy,  
Collaborative Innovation Center of IFSA (CICIFSA),  
Shanghai Jiao Tong University, Shanghai 200240, China

(Dated: June 11, 2019)

Atoms exposed to high-frequency strong laser fields experience the ionization suppression due to the deformation of Kramers-Henneberger (KH) wave functions, which has not been confirmed yet in experiment. We propose a bichromatic pump-probe strategy to affirm the existence of KH states, which is formed by the pump pulse and ionized by the probe pulse. In the case of the single-photon ionization triggered by a vacuum ultra-violet probe pulse, the double-slit structure of KH atom is mapped to the photoelectron momentum distribution. In the case of the tunneling ionization induced by an infrared probe pulse, streaking in anisotropic Coulomb potential produces a characteristic momentum drift. Apart from bichromatic schemes, the non-Abelian geometric phase provides an alternative route to affirm the existence of KH states. Following specific loops in laser parameter space, a complete spin flipping transition could be achieved. Our proposal has advantages of being robust against focal-intensity average as well as ionization depletion, and is accessible with current laser facilities.

PACS numbers: 42.50.Hz 42.65.Re 82.30.Lp

Modern light-matter interaction researches date back to Einstein’s explanation on the photoelectric effect, in which ionization happens only if an absorbed photon energy is larger than the binding energy. The advent of modern laser technologies has boosted light-matter interaction researches into new eras, where novel nonperturbative phenomena are discovered, for examples, strong-field tunneling ionization [1], above threshold ionization [2], high-harmonic generation [3–5], nonsequential double ionization [6], low energy structures [7, 8], and photoelectron holography [9] *et al.*. Among these fascinating scenarios, stabilization of atoms in intense laser fields, i.e., the counterintuitive decreasing of ionization probability with the increasing of driving laser intensities, attracts attentions of the ultrafast community [10–12].

Two mechanisms are known for stabilization. One is interference stabilization [13], in which the released electron wave packets from populated Rydberg states interfere destructively. The other is adiabatic stabilization, in which the multiphoton ionization is suppressed due to the deformation of Kramers-Henneberger (KH) wave functions [14, 15], which are defined to be the eigenstates of a time-averaged Hamiltonian [16].

Though theoretically predicted for decades, the experimental confirmation of adiabatic stabilization is obscure due to several difficulties. A realistic laser pulse has a spatial intensity distribution. While the field strength in the focused center reaches the threshold of stabilization, the lower intensity around the focusing spot may completely ionize the target. Hence, theoretical predictions were usually smeared out after focal-intensity average. Another obstacle is the ionization depletion, i.e., the target might be completely ionized before the laser field reaches its peak intensity [17]. Up to now, there is only tantalizing indirect experimental evidences for the

adiabatic stabilization. For example, in Ref. [18], a large acceleration of neutral atoms was reported and regarded as a signal of stabilization [19]. However, this evidence is not convincing enough as frustrated ionization [20], in which the ionized electrons get recaptured by the parent nuclei, has the similar output.

There are vast researches on adiabatic stabilization [10–12]. However, only few attempted to directly identify KH states. Kulander *et al.* suggested that the appearance of even order of high-harmonic generation [21] is a manifest of KH states. Morales *et al.* identified specific fine structure in photoelectron momentum distribution contributed by excited KH states [22]. Jiang *et al.* suggested that the photoelectron momentum distribution carrying dynamical interference structures provides information of adiabatic stabilization [23]. However, these proposals are sensitive either to the laser intensity or to the pulse envelope and are not robust against ionization depletion. Thus, the experiment realization is still challenging.

In this letter, we proposed to detect KH states using the bichromatic pump-probe strategy, in which the KH state is formed by the pump pulse and ionized by the probe one. By detecting the photoelectron momentum distribution, one is able to extract the dichotomic structure of the target, and thereby affirm the KH states. The spin flipping for atoms following a loop in the laser parameter space can also be used to affirm the existence of KH states.

Our start point is the three-dimensional time-dependent Schrödinger equation (TDSE) in the KH frame [16] (atomic units are used throughout unless stated otherwise)

$$i\frac{\partial}{\partial t}\psi(\mathbf{r}, t) = \left[ \frac{1}{2}\mathbf{p}^2 + V(\mathbf{r} + \boldsymbol{\beta}) \right] \psi(\mathbf{r}, t), \quad (1)$$

where  $\beta$  is the time-dependent electron displacement  $\beta = \beta_0 \sin(\omega_0 t)$ , with  $\beta_0 = \beta_0 f(t) \mathbf{e}_x$  and  $\beta_0 = \frac{E_0}{\omega^2}$  if the driving laser field is linearly polarized along the  $x$  axis. The corresponding laser field is given by  $\mathbf{E}(t) = -\frac{\partial^2}{\partial t^2} \beta$ . We use the envelope  $f(t) = \cos^2(t/L\pi)$  throughout this paper, where  $L$  stands for the pulse duration. The ground state of Eq. (1) is obtained using the imaginary time method [24], and the split-operator method is adopted to propagate the wave function in real time. By Fourier transforming the ionized wave function, we obtained the photoelectron momentum distribution. Using the hydrogen atom as the prototypical target, we calculated the ionization probability as a function of  $\beta_0$ , as shown by the black solid line in Fig. 1 (a). Here, the laser pulse has the frequency  $\omega_0 = 3$  a.u., and a total duration  $L$  of sixty cycles. The “death valley” [17] structure is clearly shown.

Researches on different aspects of high-frequency-laser ionization scatter in references [25–33], for our purpose here, we summarize the main conclusions with a special emphasis on the role played by KH states. We expanded the oscillating Coulomb potential as  $V(\mathbf{x} + \beta) \approx \sum_n V_n(\mathbf{x}; \beta_0) e^{-in\omega_0 t}$  [34, 35].  $V_0(\mathbf{x}; \beta_0)$  provides a laser-dressed adiabatic potential, while the nonzero harmonic components  $V_n(\mathbf{x}; \beta_0)$  induce photon absorption/emission. The Hamiltonian in Eq. (1) can now be regrouped into two parts, i.e., the adiabatic term  $H_0 = \frac{\mathbf{p}^2}{2} + V_0(\mathbf{r}; \beta_0)$  and the remaining part  $H_I = \sum_n V_n(\mathbf{x}; \beta_0) e^{-in\omega_0 t}$ . The time-dependent electron wave packet can be expanded as

$$\Psi(t) = \sum_N C_N(t) e^{-i \int^t d\tau E_N(\tau)} \phi_N(\beta_0), \quad (2)$$

in which  $\phi_N(\beta_0)$  is the instantaneous eigenstate of  $H_0$  and satisfies the governing equation  $H_0 |\phi_N(\beta_0)\rangle = E_N(\beta_0) |\phi_N(\beta_0)\rangle$ . Inserting Eq. (2) into the Schrödinger equation yields

$$\dot{C}_N = \sum_M \langle N | \left( -\frac{\partial \beta_0}{\partial t} \frac{\partial}{\partial \beta_0} - i H_I \right) | M \rangle e^{-i \int^t d\tau (E_M - E_N)} C_M. \quad (3)$$

The term  $\langle N | H_I | M \rangle$  is responsible for photons absorption/emission, and the skew-hermitian matrix  $\langle N | \frac{\partial}{\partial \beta_0} | M \rangle$  provides the nonadiabatic coupling [25–27] and the geometric phase [36]. As indicated by Eq. (3), KH states are of central importance here. The deformation of the KH wave function  $\phi_N(\beta_0)$  leads to the suppression of  $\langle N | V_n | M \rangle$ , which is the fundamental reason for adiabatic stabilization [14, 15]. The phase accumulation due to the distorted KH state leads to the dynamic interference [28–31]. Furthermore, KH states determine the strength of nonadiabatic coupling  $\langle N | \frac{\partial}{\partial \beta_0} | M \rangle$ .

With Eq. (3) in hand, we explored scenarios of ionization shown in Fig. 1 by dividing the ionization probability curve into three stages marked by A, B and C.

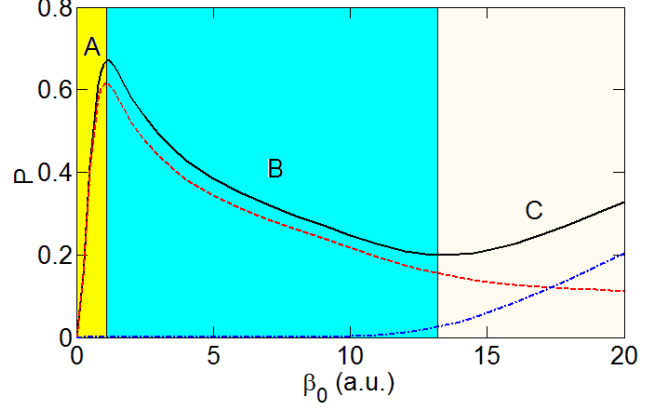


FIG. 1: The ionization probability as a function of  $\beta_0$  obtained from TDSE simulations. The black solid line is for total ionization, the red dashed line is for one-photon ionization probability, and the blue dotted-dash line describes the nonadiabatic ionization.

In stage A,  $\beta_0$  is small and so is the changing rate  $\frac{\partial \beta_0}{\partial t}$ , which means the deformation of KH wave functions and the nonadiabatic coupling are negligible. We extracted the single-photon ionization fragment from the total ionization spectra, and presented it by the red dashed curve in Fig. 1. The single-photon-ionization probability overlaps with the total ionization probability as  $\beta_0 < 1$  a.u., which suggests that the ionization can be well described by the conventional first-order perturbation theory and the nonadiabatic coupling is negligible. In stage B, the total ionization probability decreases due to the significant deformation of KH wave functions. The norm of  $\langle N | V_n | M \rangle$  is suppressed with an increasing  $\beta_0$ . The dichotomic characteristic of KH states, i.e., the dimensionless number  $\frac{Z}{\beta_0 I_p}$ , serves as a measure of the deformation of wave functions. For the ground state hydrogen atom, the nuclear charge  $Z = 1$  a.u. and the ionization energy  $I_p = 0.5$  a.u..  $\frac{Z}{\beta_0 I_p} \approx 1$  roughly corresponds to the point where the second order derivative of the laser-dressed ground state energy curve vanishes [37].  $\frac{Z}{\beta_0 I_p} < 1$  implies the deformation of wave function is significant. In stage C, the nonadiabatic ionization becomes more and more important [25–27]. There is no distinct boundary between B and C. The nonadiabatic coupling is determined by the product of  $\langle N | \frac{\partial}{\partial \beta_0} | M \rangle$  and  $\frac{\partial \beta_0}{\partial t}$ , which implies an envelope dependence. Similar to the excited-state tunneling ionization [38], in the nonadiabatic ionization, the atom first transits to excited states, which are then mediated to continuum states. The effective ionization potential decreases with the increasing of  $\beta_0$ , as shown in the supplementary file [37], and thus the nonadiabatic ionization is more important for a larger  $\beta_0$ . Ionization from excited states is dominated since the ionization energy gets smaller in this situation.

With these understandings about the central role played by KH states in the  $\omega_0 \gg I_p$  regime, we now make the following proposal to experimentally affirm KH states. The strategy is basically a pump-probe scheme: a linearly or circularly polarized high-frequency strong laser pulse is used to irradiate on a prototypical hydrogen atom, which is to be ionized by another circularly polarized probe pulse. When the electron is released from the KH hydrogen atom, who plays the role of a double-slits, the photoelectron momentum distribution will inherit the double-slit interference structure. In principle, this proposal can already be performed on advanced laser facilities [39–41]. In this strategy, the probe pulse should be strong enough to trigger noticeable ionization, but not so strong that the formed KH state gets destroyed. This imposes a constraint  $I_2 \ll (\frac{\omega_2}{\omega_1})^4 I_1$ , where  $I_1$  and  $I_2$  are intensities of the pump and probe pulses. Note that the subscript 0 is preserved for the case of using only one pulse. Besides that, laser frequencies of the pump and probe pulses should be proper so that the photoelectron momentum distribution induced by the pump and probe pulses does not overlap.  $\omega_2$  should be sufficiently large to avoid interfering with very low energy electron produced by nonadiabatic coupling [25, 26].

The upper row of Fig. 2 shows the above-threshold-ionization (ATI) containing the fragments released by absorbing  $n\omega_1$  photons and  $m\omega_2$  photons, where  $n$  and  $m$  are integers. Though the probability of absorbing  $\omega_2$  is small due to the relative weak intensity of the probe pulse, the ionization by the probe pulse contributes distinguished angular distribution and non-overlapping photoelectron energy with the ionization fragments induced by the pump pulse. Thus one can easily separate one-probe-photon ionization from the dominating pump-photon ionization, as shown in the lower row in Fig. 2. The laser parameters for the three columns are presented in the caption. The ionization amplitude of formed KH states, with the field parameters used in (d), is proportional to  $J_n(p_x A_1/\omega_1) J_{m+1}(\sqrt{p_x^2 + p_y^2} A_2/\omega_2) + J_n(p_x A_1/\omega_1) J_{m-1}(\sqrt{p_x^2 + p_y^2} A_2/\omega_2)$ , where  $J_n$  is the  $n$ -th order Bessel function [37]. All panels in the lower row present clearly angular nodal structures, which are the manifestation of double-slit interference [42]. The number of nodes is determined by  $\beta_1 \sqrt{2E_k}$  with  $E_k$  the photoelectron energy. Inversely,  $\beta_1$  can be extracted from the angular distribution of the photoelectron induced by the one-probe-photon ionization. The comparison of (a), (b) and (c) shows that a larger  $\omega_1$  is more convenient for separating the ionization events from the pump and probe pulses. A higher frequency  $\omega_1$  is also better for avoiding ionization depletion [43].

The unavoidable focal-intensity average in real experiments must be taken into account to judge the feasibility of the above proposal. By assuming that the intensity of the laser pulse has the spatially Gaussian distribution

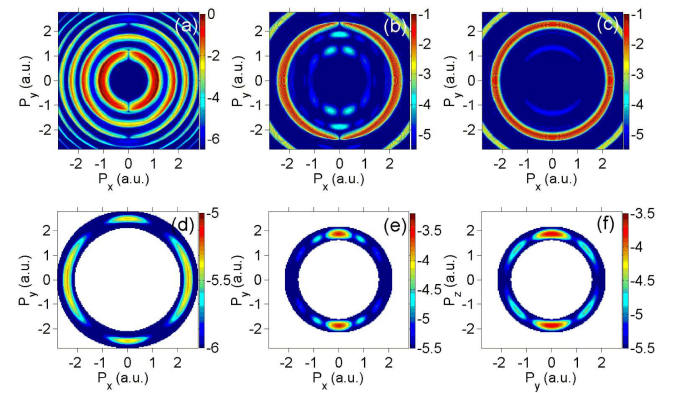


FIG. 2: Upper row: The photoelectron momentum distributions contributed by both the pump and probe pulses. Lower row: The photoelectron momentum distributions contributed by the one-probe-photon ionization, which are picked out from the upper row. Different laser parameters are used for the three columns. Left column:  $\beta_1 = 2$  a.u.,  $\omega_1 = 1$  a.u., and  $\omega_2 = 3.5$  a.u.; The pump pulse is linearly polarized along the  $x$  axis with a duration of twenty optical cycles, and the probe pulse is circularly polarized in the  $x-y$  plane. Middle column:  $\beta_1 = 5$  a.u.,  $\omega_1 = 3$  a.u., and  $\omega_2 = 2$  a.u.; The pump pulse is linearly polarized along the  $x$  axis with a duration of sixty optical cycles, and the probe pulse is circularly polarized in the  $x-y$  plane. Right Column:  $\beta_1 = 3$  a.u.,  $\omega_1 = 3$  a.u., and  $\omega_2 = 2$  a.u.; The pump pulse is circularly polarized in the  $x-y$  plane with a duration of sixty optical cycles, and the probe pulse is circularly polarized in the  $y-z$  plane. In the all panels, the probe pulse has a duration of ten optical cycles and intensity  $I_2 = 10^{16}$  W/cm<sup>2</sup>. The delay between the pump and probe pulses is zero.

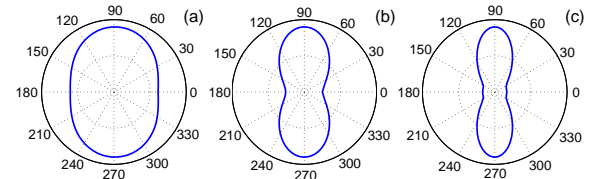


FIG. 3: Focal-intensity averaged photoelectron angular distributions. The laser frequencies are  $\omega_1 = 1$  a.u., and  $\omega_2 = 3.5$  a.u.. The pump laser intensity is (a)  $I_1 = 3.5 \times 10^{16}$  W/cm<sup>2</sup> ( $\beta_1 = 1$  a.u. ), (b)  $I_1 = 1.4 \times 10^{17}$  W/cm<sup>2</sup> ( $\beta_1 = 2$  a.u. ), and (c)  $I_1 = 3.2 \times 10^{17}$  W/cm<sup>2</sup> ( $\beta_1 = 3$  a.u.). The probe laser has the intensity  $I_2 = 1 \times 10^{16}$  W/cm<sup>2</sup>, and the duration of ten optical cycles.

[44], we plotted the focal-intensity-averaged photoelectron angular distribution in Fig. 3. The frequencies are  $\omega_1 = 1$  a.u. and  $\omega_2 = 3.5$  a.u., corresponding to the parameters used in Fig. 2 (a)(d). The laser intensities used for the three columns from left to right are  $I_1 = 3.5 \times 10^{16}$  W/cm<sup>2</sup> ( $\beta_1 = 1$  a.u. ),  $I_1 = 1.4 \times 10^{17}$  W/cm<sup>2</sup> ( $\beta_1 = 2$  a.u. ), and  $I_1 = 3.2 \times 10^{17}$  W/cm<sup>2</sup> ( $\beta_1 = 3$  a.u. ), respectively. The photoelectron from unperturbed hydrogen

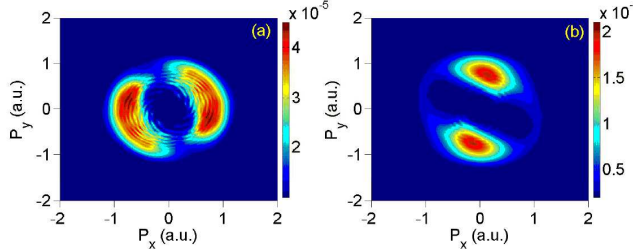


FIG. 4: Focal-intensity-averaged photoelectron momentum distributions that are tunneling ionized by infrared probe pulses. The pump and probe laser intensities are (a)  $\beta_1 = 2$  a.u. and  $I_2 = 3 \times 10^{14}$  W/cm<sup>2</sup>, and (b)  $\beta_1 = 4$  a.u. and  $I_2 = 2 \times 10^{14}$  W/cm<sup>2</sup>. The probe pulse has the duration of four optical cycles.

atom should be rotational invariant in the laser polarization plane, hence, the anisotropic ionization probability, as shown in all these panels, confirms the existence of dichotomic distribution of the KH hydrogen atom, which in turn provides the evidence of adiabatic stabilization. The onset of adiabatic ionization implies that ionization is mainly contributed from small  $\beta_1$  [37], which explains the fact that interference structures in photoelectron momentum distribution are not that distinct as Fig. 2. As the number of nodes is determined by  $\beta_1\sqrt{2E_k}$ , a larger  $\omega_2$  is favored to produce distinctive angular distributions. This strategy works for diverse laser parameters and is robust against focal-intensity average. Moreover, the pump-probe delay can be tuned thus the probe pulse can contribute the noticeable ionization before the KH atom is depleted.

Instead of the single-photon ionization by the high-frequency probe pulse, the KH atom may be tunneling ionized by an infrared probe pulse. Figure 4 shows the focal-volume-averaged photoelectron momentum distributions for the probe laser intensity (a)  $I_2 = 3 \times 10^{14}$  W/cm<sup>2</sup> and  $\beta_1 = 2$  a.u. and (b)  $I_2 = 2 \times 10^{14}$  W/cm<sup>2</sup> and  $\beta_1 = 4$  a.u.. Here, He<sup>+</sup> is used as the target, and the two cases have the same Keldysh parameter. In contrast to the one-probe-photon ionization, signals from large  $\beta_1$  is dominating in tunneling regime [37].

The streaking of the photoelectron momentum distribution in the anisotropic Coulomb field produces a tilt angle, which is a function of  $\beta_1$  and  $I_2$  [45, 46]. The existence of  $\beta_1$  is thus mapped into the streaking tilt an-

gle. We point out that it is also possible to use the laser induced electron diffraction [47, 48] or charge resonance enhanced ionization [49] to reconstruct  $\beta_1$  [37].

Besides utilizing the double-slit interference structure and the anisotropic angular streaking, the electron spin flipping provides another route to affirm KH atoms. The physical principle is based on the non-Abelian geometric phase. Neglecting the ionization of KH atoms for a moment, the nonadiabatic coupling among those non-degenerate states, i.e.,

$$\langle N | \frac{\partial}{\partial \beta_0} | M \rangle = \langle N | \frac{\partial H_0}{\partial \beta_0} | M \rangle / (E_M - E_N), \quad (4)$$

could be suppressed in the adiabatic limit. However, situations are different for systems with the energy degeneracy, where non-Abelian geometric phases play a role [50]. Denoting the polarization axis of the laser pulse by  $\mathbf{n} = (\sin \theta \cos \phi, \sin \theta \sin \phi, \cos \theta)$ , we have degenerate KH states  $|\pm(\theta, \phi)\rangle$  satisfying  $\mathbf{n} \cdot \mathbf{J} |\pm(\theta, \phi)\rangle = \pm 1/2 |\pm(\theta, \phi)\rangle$ . Where  $\mathbf{J}$  is the addition of orbital angular momentum  $\mathbf{L}$  and spin angular momentum  $\mathbf{S}$ .

$|\pm(\theta, \phi)\rangle$  are connected to  $|\pm(\theta = 0, \phi = 0)\rangle$  via rotations

$$|\pm(\theta, \phi)\rangle = \exp(-iJ_z\phi) \exp(-iJ_y\theta) |\pm(\theta = 0, \phi = 0)\rangle. \quad (5)$$

Components of non-Abelian connection 1-form  $\mathfrak{A} = i \langle M | \mathbf{d} | N \rangle$ , where  $\mathbf{d}$  is exterior derivative, are thus given by

$$\mathfrak{A}_\theta = \frac{1}{2} \begin{pmatrix} 0 & -i\kappa \\ i\kappa & 0 \end{pmatrix}, \quad \mathfrak{A}_\phi = \frac{1}{2} \begin{pmatrix} \cos \theta & -\sin \theta \kappa \\ -\sin \theta \kappa & -\cos \theta \end{pmatrix}. \quad (6)$$

Here  $\kappa = 2 \langle +(\theta = 0, \phi = 0) | J_x | -(\theta = 0, \phi = 0) \rangle$  is a real valued function of  $\beta_0$ , up to a trivial phase factor. We have  $\kappa = 1$  when  $\beta_0 \rightarrow 0$ . And in the limit  $\beta_0 \rightarrow \infty$ ,  $\kappa = 0$  if we choose  $|+(\theta = 0, \phi = 0)\rangle = |L_z = 1, S_z = -1/2\rangle$  and  $|-(\theta = 0, \phi = 0)\rangle = |L_z = -1, S_z = 1/2\rangle$ . Such a choice is possible here, as the off-diagonal elements of spin-orbital coupling matrix vanish.

Consider the situation that the laser field is linearly polarized along  $z$  axis. Adiabatically rotates the polarization axis by  $\theta_0 = \pi/2$  in the  $z - x$  plane, then rotates it by  $\phi_0$  in  $x - y$  plane, and finally rotates it back to the  $z$  axis. The holonomy  $W = P \left\{ e^{i \oint \mathfrak{A}} \right\}$  for such a closed path is

$$W = \begin{pmatrix} \cos \left( \frac{\kappa \phi_0}{2} \right) + i \sin \left( \frac{\kappa \pi}{2} \right) \sin \left( \frac{\kappa \phi_0}{2} \right) & -i \cos \left( \frac{\kappa \pi}{2} \right) \sin \left( \frac{\kappa \phi_0}{2} \right) \\ -i \cos \left( \frac{\kappa \pi}{2} \right) \sin \left( \frac{\kappa \phi_0}{2} \right) & \cos \left( \frac{\kappa \phi_0}{2} \right) - i \sin \left( \frac{\kappa \pi}{2} \right) \sin \left( \frac{\kappa \phi_0}{2} \right) \end{pmatrix}. \quad (7)$$

By setting  $\phi_0 = \pi/\kappa$ , we have the spin flipping tran-

sition amplitude  $-i \cos \left( \frac{\kappa \pi}{2} \right)$ , which is forbidden when

$\kappa = 1$  and maximal when  $\kappa$  approaches zero.

The deformation of KH state is crucial here. When the laser field is not strong, i.e.  $\beta_0 < 1$  a.u., the dynamical evolution of TDSE is governed by the dipole coupling matrix  $\langle N | \mathbf{r} | M \rangle$ . Typically, only a minor fraction of spin flipping could be achieved [51]. However, with an increasing  $\beta_0$ , couplings with the oscillating laser pulses are suppressed, reducing Eq. (3) into

$$\frac{\partial C_N}{\partial \beta_0} \approx - \sum_{E_M=E_N} \langle N | \frac{\partial}{\partial \beta_0} | M \rangle C_M \quad (8)$$

in the adiabatic limit.

This is an atomic realization of the rotation effect studied in diatomic molecule [52]. The adiabatically rotating electric field is isomorphic to the rotating molecule axis. The nontrivial value  $\kappa \neq 1$  manifests the breaking of atomic isotropic symmetry thus the existence axial symmetric KH atom. In this strategy, ensuring the adiabaticity implies that  $\frac{\partial \beta_0}{\partial t}$  should be small. Therefore, a pulse with a very long duration is demanded. In this case, in order to avoid ionization depletion, a laser pulse with large  $\omega_0$  is required.

To summarize, a pump-probe scheme is suggested to detect the KH state. The pump pulse creates a KH atom, whose dichotomic structure is imprinted on the photoelectron momentum distribution. This strategy is robust against the focal-intensity average and ionization depletion. Alternatively, the spin flipping induced by the non-Abelian geometric phase in the adiabatically changing laser field can also provide an evidence of KH atoms. An ideal implementation of our proposal requires  $\frac{\omega_1}{I_p} > 1$  and  $\frac{Z}{\beta_1 I_p} < 1$ . In our strategy, the required laser intensity is about  $I_1 = 10^{16} - 10^{17}$  W/cm<sup>2</sup>, and the laser wavelength is around 10–50 nm, which is within the reach of current laser facilities. Relativistic and QED effects [53, 54] are negligible for the considered laser parameters. Moreover, we are concerned only about one-probe-photon ionization from KH states, thus the deviation from relativistic theory mainly differs by scaling factors [55]. Our schemes not only provide accessible routes for detecting KH states, thus adiabatic stabilization, but are also useful for understanding up-coming high frequency strong laser experimental results.

This work was supported by National Key R&D Program of China (2018YFA0404802), Innovation Program of Shanghai Municipal Education Commission(2017-01-07-00-02-E00034), National Natural Science Foundation of China (NSFC) (Grant No. 11574205, 11721091, 91850203), and Shanghai Shuguang Project (17SG10). Simulations were performed on the  $\pi$  supercomputer at Shanghai Jiao Tong University.

<sup>†</sup> Electronic address: fhe@sjtu.edu.cn

- [1] M. Uiberacker, T. Uphues, M. Schultze M, *et al.*, Attosecond real-time observation of electron tunnelling in atoms, *Nature*, **446**, 627 (2007).
- [2] P. Agostini, F. Fabre, G. Mainfray, G. Petit, and N. K. Rahman, Free-free transitions following six-photon ionization of xenon atoms, *Phys. Rev. Lett.* **42**, 1127 (1979).
- [3] A. L'Huillier and P. Balcou, *Phys. Rev. Lett.* **70**, 774 (1993).
- [4] P. B. Corkum, Plasma perspective on strong field multi-photon ionization, *Phys. Rev. Lett.* **71**, 1994 (1993).
- [5] S. Ghimire, A. D. DiChiara, E. Sistrunk, *et al.*, Observation of high-order harmonic generation in a bulk crystal, *Nat. Phys.* **7**, 138 (2011).
- [6] A. L'Huillier, L. A. Lompre, G. Mainfray, *et al.*, Multiply charged ions induced by multiphoton absorption in rare gases at 0.53  $\mu$ m, *Phys. Rev. A* **27**, 2503 (1983).
- [7] C. I. Blaga, F. Catoire, P. Colosimo, *et al.*, Strong-field photoionization revisited, *Nat. Phys.* **5**, 335 (2009).
- [8] W. Quan, Z. Lin, M. Wu, *et al.*, Classical aspects in above-threshold ionization with a midinfrared strong laser field, *Phys. Rev. Lett.* **103**, 093001 (2009).
- [9] Y. Huismans, A. Rouzée, A. Gijsbertsen, *et al.*, Time-resolved holography with photoelectrons, *Science* **331**, 61 (2011).
- [10] M. Gavrila, Atomic stabilization in superintense laser fields, *J. Phys. B: At Mol. Opt. Phys.* **35**, R147 (2002).
- [11] A. M. Popov, O. V. Tikhonova, E. A. Volkova, Strong-field atomic stabilization: numerical simulation and analytical modelling, *J. Phys. B: At Mol. Opt. Phys.* **36**, R125 (2003).
- [12] M. Richter, Imaging and controlling electronic and nuclear dynamics in strong laser fields. (Ph.D. Thesis, Technischen Universität Berlin, 2016)
- [13] M. V. Fedorov and A. M. Movsesyan, Field-induced effects of narrowing of photoelectron spectra and stabilisation of Rydberg atoms, *J. Phys. B: At. Mol. Opt. Phys.* **21**, L155 (1988).
- [14] M. Pont, and M. Gavrila, Stabilization of atomic hydrogen in superintense, high-frequency laser fields of circular polarization, *Phys. Rev. Lett.* **65**, 2362 (1990).
- [15] J. H. Eberly, K. C. Kulander, Atomic stabilization by super-intense lasers, *Science* **262**, 1229 (1993).
- [16] W. C. Henneberger, Perturbation method for atoms in intense laser fields, *Phys. Rev. Lett.* **21**, 838 (1968).
- [17] P. Lambropoulos, Mechanisms for multiple ionization of atoms by strong pulsed lasers, *Phys. Rev. Lett.* **55**, 2141 (1985).
- [18] U. Eichmann, T. Nubbemeyer, H. Rottke, and W. Sandner, Acceleration of neutral atoms in strong short-pulse laser fields, *Nature* **461**, 1261 (2009).
- [19] Q. Wei, P. Wang, S. Kais, and D. Herschbach, Pursuit of the Kramers-Henneberger atom, *Chem. Phys. Lett.* **683**, 240 (2017).
- [20] T. Nubbemeyer, K. Gorling, A. Saenz, U. Eichmann, and W. Sandner, Strong-field tunneling without ionization, *Phys. Rev. Lett.* **101**, 233001 (2008).
- [21] K. C. Kulander, K. J. Schafer, and J. L. Krause, Dynamic stabilization of hydrogen in an intense, high-frequency, pulsed laser field, *Phys. Rev. Lett.* **66**, 2601 (1991).
- [22] F. Morales, M. Richter, S. Patchkovskii, and O. Smirnova, Imaging the Kramers-Henneberger atom, *Proc. Natl. Acad.* **108**, 16906 (2011).
- [23] W. C. Jiang, and J. Burgdörfer, Dynamic interference as

\* Electronic address: a225633@sjtu.edu.cn

signature of atomic stabilization, *Opt. Express* **26**, 19921 (2018).

[24] R. Kosloff, and H. Tal-Ezer, A direct relaxation method for calculating eigenfunctions and eigenvalues of the Schrödinger equation on a grid, *Chem. Phys. Lett.* **127**, 223 (1986).

[25] M. Førre, S. Selstø, J. P. Hansen, and L. B. Madsen, Exact nondipole Kramers-Henneberger form of the light-atom Hamiltonian: an application to atomic stabilization and photoelectron energy spectra, *Phys. Rev. Lett.* **95**, 043601 (2005).

[26] K. Toyota, O. I. Tolstikhin, T. Morishita, *et al.*, Slow electrons generated by intense high-frequency laser pulses, *Phys. Rev. Lett.* **103**, 153003 (2009).

[27] Q. C. Ning, U. Saalmann, and J. M. Rost, Electron dynamics driven by light-pulse derivatives, *Phys. Rev. Lett.* **120**, 033203 (2018).

[28] P. V. Demekhin and L. S. Cederbaum, Dynamic interference of photoelectrons produced by high-frequency laser pulses, *Phys. Rev. Lett.* **108**, 253001 (2012).

[29] P. V. Demekhin and L. S. Cederbaum, ac Stark effect in the electronic continuum and its impact on the photoionization of atoms by coherent intense short high-frequency laser pulses, *Phys. Rev. A* **88**, 043414 (2013).

[30] M. Baghery, U. Saalmann, and J. M. Rost, Essential conditions for dynamic interference, *Phys. Rev. Lett.* **118**, 143202 (2017).

[31] M. X. Wang, H. Liang, X. R. Xiao, *et al.*, Nondipole effects in atomic dynamic interference, *Phys. Rev. A* **98**, 023412 (2018).

[32] M. Pont, N. R. Walet, M. Gavrila, and C. W. McCurdy, Dichotomy of the hydrogen atom in superintense, high-frequency laser fields, *Phys. Rev. Lett.* **61**, 939 (1988).

[33] M. Pont, Atomic distortion and ac-Stark shifts of H under extreme radiation conditions, *Phys. Rev. A* **40**, 5659.

[34] G. Yao, and R. E. Wyatt, Stationary approaches for solving the Schrödinger equation with time-dependent Hamiltonians, *J. Chem. Phys.* **101**, 1904 (1994).

[35] K. Toyota, U. Saalmann, and J. M. Rost, The envelope Hamiltonian for electron interaction with ultrashort pulses, *New J. Phys.* **17**, 073005 (2015).

[36] M. V. Berry, Quantal phase factors accompanying adiabatic changes, *Proc. Roy. Soc. London, Ser. A* **392**, 45 (1984).

[37] See the supplemental materias.

[38] E. E. Serebryannikov, and A. M. Zheltikov, Strong-field photoionization as excited-state tunneling, *Phys. Rev. Lett.* **116**, 123901.

[39] A. A. Sorokin, S. V. Bobashev, T. Feigl, *et al.*, Photoelectric effect at ultrahigh intensities, *Phys. Rev. Lett.* **99**, 213002 (2007).

[40] M. Fuchs, M. Trigo, J. Chen, *et al.*, Anomalous nonlinear X-ray Compton scattering, *Nat. Phys.* **11**, 964 (2015).

[41] S. Huang, Y. Ding, Y. Feng, *et al.*, Generating single-spike hard X-ray pulses with nonlinear Bunch compression in free-electron lasers, *Phys. Rev. Lett.* **119**, 154801 (2017).

[42] M. Kunitski, N. Eicke, P. Huber, J. Köhler, *et al.*, Double-slit photoelectron interference in strong-field ionization of the neon dimer, *Nat. Comm.* **10**, 1 (2019).

[43] J. Grochmalicki, M. Lewenstein, K. Rzaewski, Stabilization of atoms in superintense laser fields: is it real?, *Phys. Rev. Lett.* **66**, 1038 (1991).

[44] A. S. Alnaser, X. M. Tong, T. Osipov, *et al.*, Laser-peak-intensity calibration using recoil-ion momentum imaging, *Phys. Rev. A* **70**, 023413 (2004).

[45] M. Odenweller, N. Takemoto, A. Vredenborg, *et al.*, Strong field electron emission from fixed in space  $H_2^+$  ions, *Phys. Rev. Lett.* **107**, 143004 (2011).

[46] P. L. He, N. Takemoto, and F. He, Photoelectron momentum distributions of atomic and molecular systems in strong circularly or elliptically polarized laser fields, *Phys. Rev. A* **91**, 063413 (2015).

[47] M. Meckel, D. Comtois, D. Zeidler *et al.*, Laser-induced electron tunneling and diffraction, *Science* **320**, 1478 (2008).

[48] C. I. Blaga, J. Xu, A. D. DiChiara *et al.*, Imaging ultrafast molecular dynamics with laser-induced electron diffraction, *Nature* **483**, 194 (2012).

[49] N. Takemoto and A. Becker, Multiple ionization bursts in laser-driven hydrogen molecular ion, *Phys. Rev. Lett.* **105**, 203004 (2010).

[50] F. Wilczek, and A. Zee, Appearance of gauge structure in simple dynamical systems, *Phys. Rev. Lett.* **52**, 2111 (1984).

[51] P. L. He, D. Lao, and F. He, Strong field theories beyond dipole approximations in nonrelativistic regimes, *Phys. Rev. Lett.* **118**, 163203 (2017).

[52] J. Moody, A. Shapere, and F. Wilczek, Realizations of magnetic-monopole gauge fields: Diatoms and spin precession, *Phys. Rev. Lett.* **56**, 893 (1986).

[53] F. Ehlotzky, K. Krajewska, and J. Z. Kamiński, Fundamental processes of quantum electrodynamics in laser fields of relativistic power, *Rep. Prog. Phys.* **72**, 046401 (2009).

[54] A. Di Piazza, C. Müller, K. Z. Hatsagortsyan and C. H. Keitel, Extremely high-intensity laser interactions with fundamental quantum systems, *Rev. Mod. Phys.* **84**, 1177 (2012).

[55] I. V. Ivanova, V. M. Shabaev, D. A. Telnov, *et al.*, Scaling relations of the time-dependent Dirac equation describing multiphoton ionization of hydrogenlike ions, *Phys. Rev. A* **98**, 063402 (2018).